Supporting Information : Local Immiscibility Control on Shape and Size of Nano-Objects in Solvo-Thermal Process: Implications for Ferroelectric Nano-Particles

Christine Bogicevic* and Pierre-Eymeric Janolin*

Université Paris-Saclay, CentraleSupélec, CNRS, laboratoire SPMS, 91190 Gif-sur-Yvette, France

E-mail: christine.bogicevic@centralesupelec.fr; pierre-eymeric.janolin@centralesupelec.fr

Additional SEM images of the $BaTiO_3$ nano-objects

In addition to Fig.3, Fig.S1 presents in a matrix form the synthesized $BaTiO_3$ nano-objects, each row corresponding to a solvent (ExW100 $- x$) and each column to the maximum temperature of the synthesis, held for 24 h. Note that the scale is different from the one used in Fig.3, except for 250-E0W100.

X-ray characterisation of $BaTiO_3$

The X-ray patterns for $BaTiO_3$ synthesized with different solvent compositions at a) 150, b) 200 and c) 250°C for 24 hours are presented in Fig.S2. X-ray diffraction was carried out on as-obtained samples, that is without acidic treatment that is used to eliminate remaining $BaCO_3$.[1] As can be seen from Fig.S2 at $2\theta \approx 24°$, traces of $BaCO_3$ appear on some of the diffractograms. On the contrary, the $Na_2Ti_3O_4$ peak at $2\theta \approx 25°$ is absent, coherently with

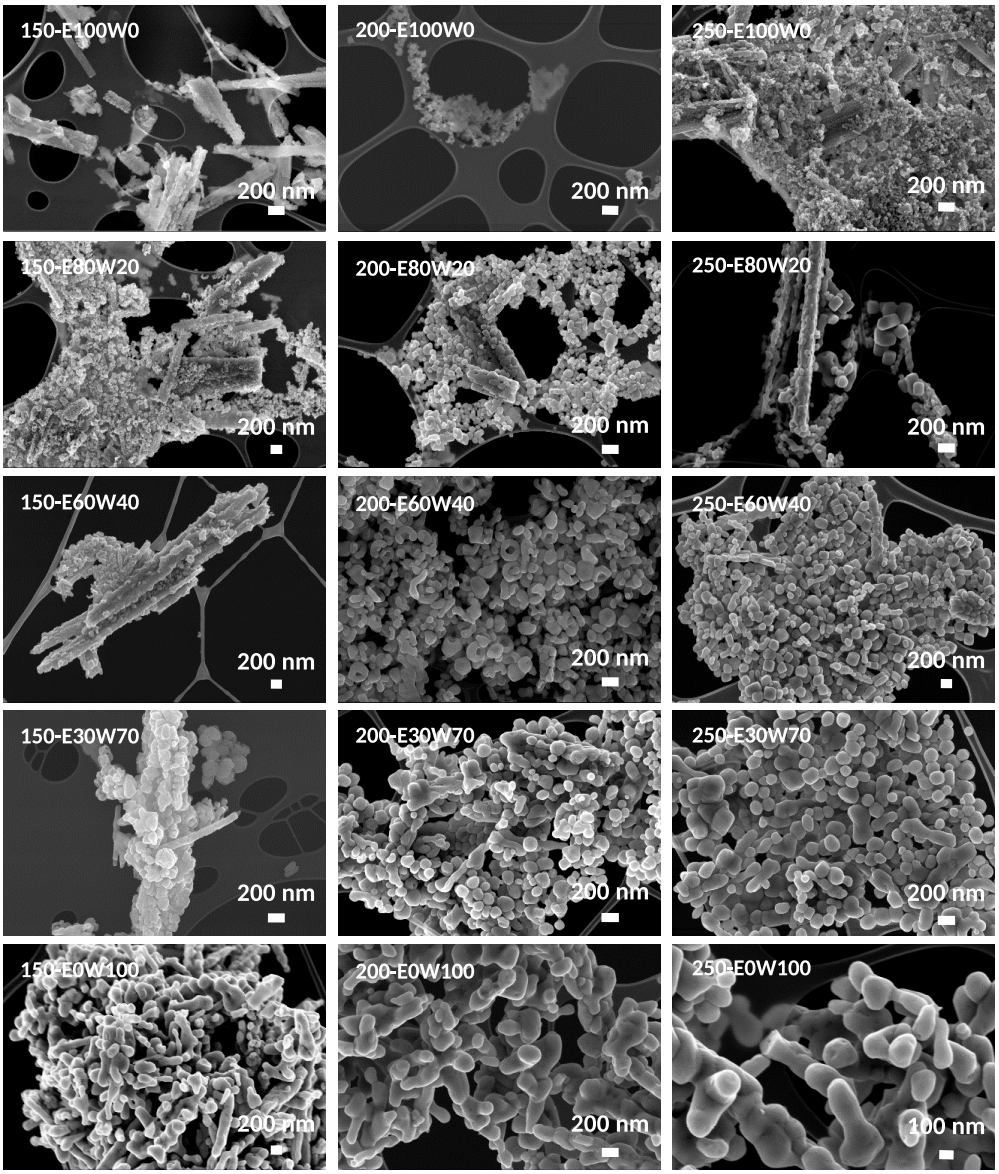

Figure S1: SEM images of the as-prepablack $BaTiO_3$ products obtained after 24 hours at 150°C (left column), 200°C (middle column), and 250°C (right column) for the various solvent compositions. This figures supplements Fig.3 with images at a different magnification (except for 250-E0W100).

the use of an initial Ba/Ti ratio of 1.1 to ensure that the $BaTiO_3$ product are not sub-stoichiometric.

Molarity of the solvents

The molarity of the ethanol-water solvents with a volume fraction Wx of water (EyWx with y=100-x) is calculated using Eq.(S1) where 0.1 is the molarity in 100% water volume, 1.44×10^{-2} is the volume fraction of water coming from the $8H_2O$ of barium hydroxide and Wx the water volume fraction of each mixture (Wx=0, 20, 40, 70 and 100).

$$M = \frac{0.1\,(100 + 1.44 \times 10^{-2})}{\mathrm{W}x} \tag{S1}$$

The resulting molarities are reported in Table.S1

Table S1: Molarity M of each solvent compositions relative to their water volume content.

	E0W100	**E30W70**	**E60W40**
M	0.1	0.14	0.25
	E80W20	**E100W0**	
M	0.5	7	

Size determination: comparison of the apparent crystallite and grain sizes

X-ray diffraction, through the Scherrer formula, provides an estimation of the apparent crystallite size, whereas SEM images enable to measure the size of the nano-objects.

The individual particle sizes were determined from the SEM images by hand, measuring the size of the particles intersecting horizontal lines (about 30 particles per line). The anisotropy was taken into account by reporting the longest of the two dimensions for elongated forms. The apparent crystallite size was calculated from the FWHM of the (111) peak (as it is a singlet in diffraction patterns of materials with a tetragonal symmetry) through

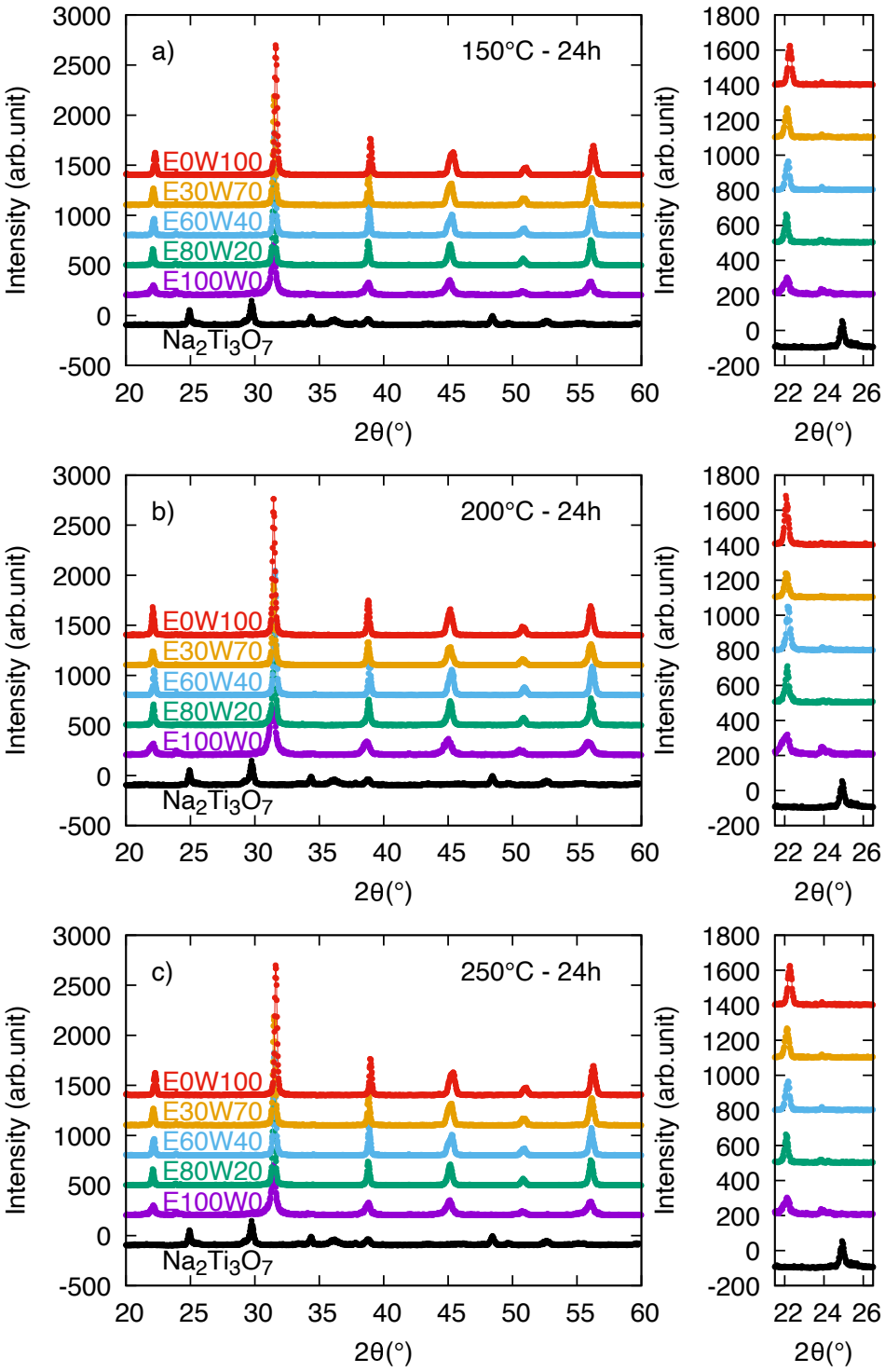

Figure S2: XRD patterns of $BaTiO_3$ synthesized with different solvent compositions at a) 150, b) 200 and c) 250°C for 24 hours. The right-hand panels are an expanded view of the range of diffraction angles where $BaCO_3$ and $Na_2Ti_3O_4$ have each one of their main peaks.

the Scherrer formula, fitted with Pseudo-Voigt profiles for Cu K_{α_1} and K_{α_2} wavelengths with a polynomial background (see Fig.S3).

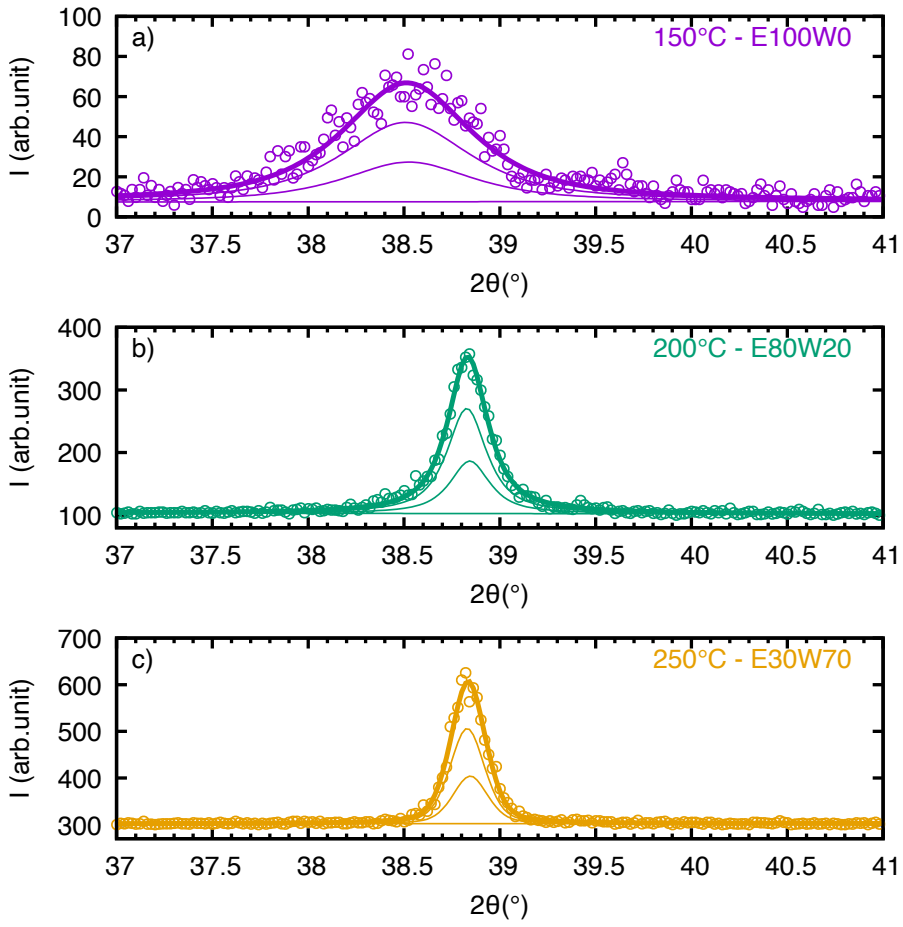

Figure S3: Representative fits (thick line) of the (111) peak with Pseudo-Voigt profiles for the Cu K_{α_1} and K_{α_2} wavelengths and a polynomial background (thin lines), for the nano-objects synthesized a) at 150°C in pure ethanol (E100W0), b) 200°C in E80W20, c) 250°C in E30W70.

The instrumental width was taken into account in the calculation of the broadening b of the Scherrer formula through $b = \sqrt{\mathrm{FWHM}^2 - \mathrm{Instr}^2}$ when the Pseudo-Voigt profile was mainly Gaussian and through $b = \mathrm{FWHM} - \mathrm{Instr}$, when the Pseudo-Voigt profile was mainly Lorentzian, with FWHM the full width at half maximum of the fitted peak and Instr the instrumental width at that angle (calculated from Caglioti parameters fitted on a reference LaB_6 sample). The relative difference between a Gaussian or Lorentzian correction ($|b_G - b_L|/[(b_G + b_L)/2]$) is of less than 1% for wide peaks (as in Fig.S3a) and naturally

larger, 6-8%, for narrower peaks (e.g. Fig.S3b and c).

Overall, taking into account the fitting uncertainty and the maximum error made on the broadening term (but neglecting errors on the wavelength and on the instrumental width) the apparent crystallite size value has a maximum uncertainty of about 10%.

Calculated from the FWHM, this "apparent crystallite" size has no obvious physical interpretation.[2] In order to determine a dimension that would better correspond to the actual dimensions of the nano-object, a thorough analysis should be carried out, using at least a more physically meaningful definition of the broadening (e.g. the integral breadth), the orientation of the crystalline planes with respect to the morphology of the nano-objects, an expression of the Scherrer constant depending on the consideblack peak and overall shape of the nano-particle, as well as the crystallite-size distribution.

The Scherrer formula, though often used in a way similar to the one reported here, can therefore only provides an estimation of the apparent crystallite size that should not be mistaken for the actual grain size.

Both size measurements give similar results for the $BaTiO_3$ nano-particles obtained with the solvent compositions E100W0 and E80W20 because they are isotropic (i.e close to spherical) and very small. For the solvent composition E60W40 the results at 250°C differ, the obtained $BaTiO_3$ nano-cubes having a large size distribution (Figure S4). With the other solvent compositions (E30W70 and E0W100) Scherrer and SEM size measurements differ as the nano-particles are larger and the obtained shapes are more anisotropic, especially with the solvent E0W100. This substantial difference between the two types of size measurement is indicated by a vertical dash line in Figure S4.

Synthesis of $BaTiO_3$ in the E0W100 solvent with a molarity of 0.25 M

The X-ray diagram of $BaTiO_3$ synthesized in E0W100 with an additional amount of barium precursor to obtain a molarity (0.25 M) corresponding to the molarity in the E60W40 solvent

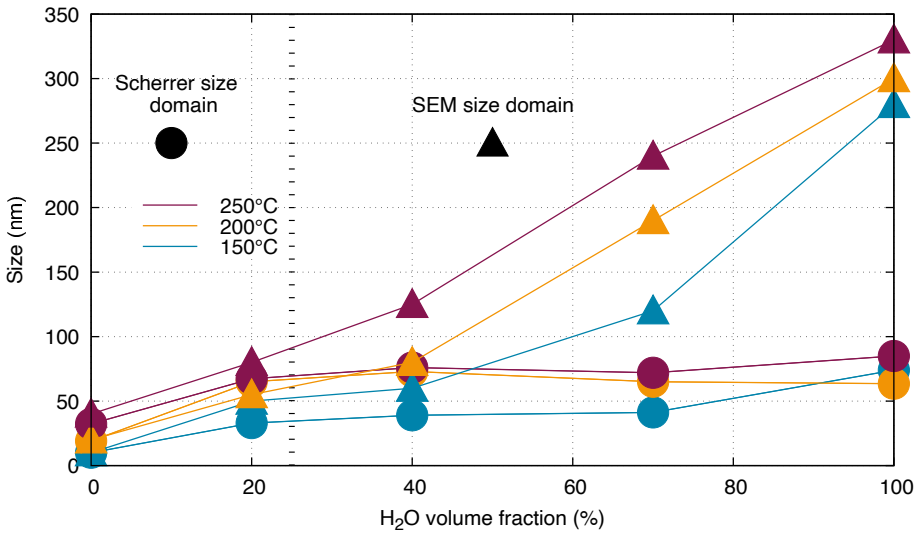

Figure S4: $BaTiO_3$ nano-particles sizes calculated by the Scherrer formula (plain circles) and measublack on the SEM images (plain triangles) for all the solvent compositions at 150°C (blue), 200°C (yellow) and 250°C (purple). The vertical dash line corresponds to a threshold where the Scherrer and SEM size measurements differ.

with the normal amount of barium precursor is shown in Figure S5. Traces of $BaCO_3$ are present at 150°C but disappear at higher temperature. This sample, as all others, exhibits the expected room-temperature tetragonal phase of $BaTiO_3$.

Ethanol volume fraction vs ethanol molar fraction

The ethanol molar fraction x_{EtOH} can be calculated using Eq.(S2),

$$x_{EtOH} = \frac{\frac{\rho_E V_E}{M_E}}{\frac{\rho_E V_E}{M_E} + \frac{\rho_W V_W}{M_W}} \tag{S2}$$

with ρ_E and ρ_W the densities, V_E and V_W the volume fractions (%) and M_E and M_W molar masses of ethanol and water respectively. The Figure S6 shows the relationship between the ethanol volume fraction and the ethanol molar fraction for the various solvents used in this study.

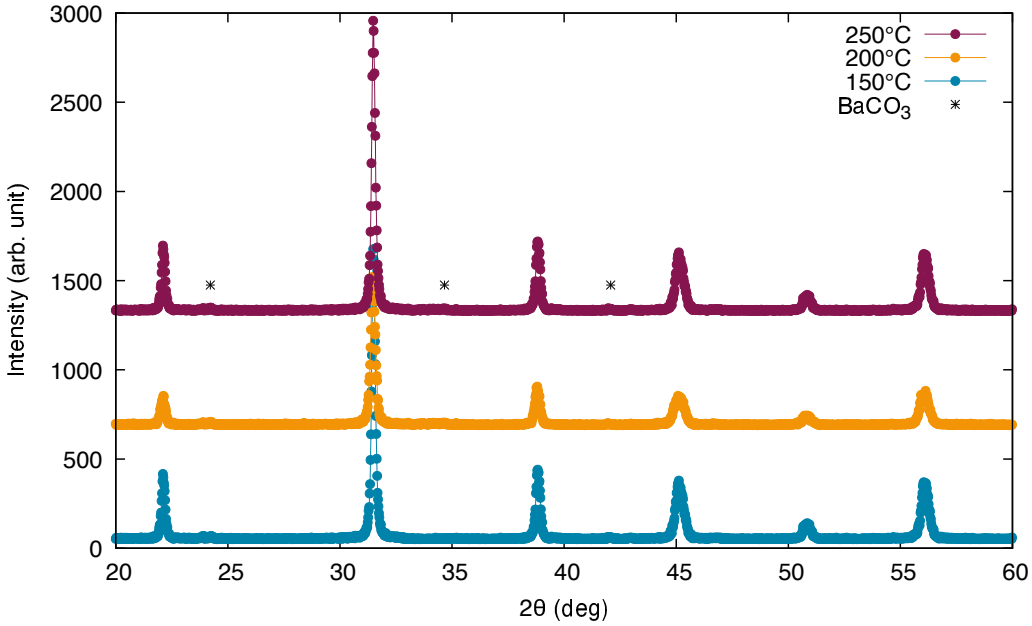

Figure S5: X-ray diagrams for $BaTiO_3$ synthesized with an additional amount of barium precursor at 150°C (blue line), 200°C (yellow), and 250°C (purple) in E0W100 to obtain a molarity of 0.25M.

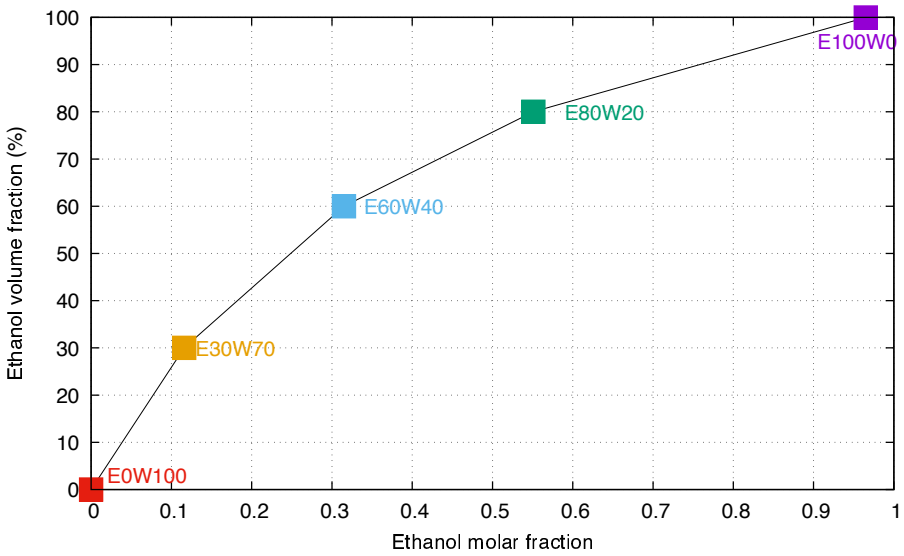

Figure S6: Ethanol volume fraction (%) vs the ethanol molar fraction x_{EtOH}.

Variation of the permittivity of the solvents as a function of temperature

The decrease of permittivity with increasing molar fraction of ethanol (x_{EtOH}) is presented on Fig.S7 (top panel) for two temperatures: 20° and 80°C. The relative difference ($\frac{\epsilon_r^0(80°\mathrm{C})-\epsilon_r^0(20°\mathrm{C})}{\epsilon_r^0(20°\mathrm{C})}$) is presented on the bottom panel of Fig.S7. A 60° increase in temperature leads to a relative decrease of ϵ_r^0 between 25 and 35%, the higher the ethanol molar fraction, the larger the difference.

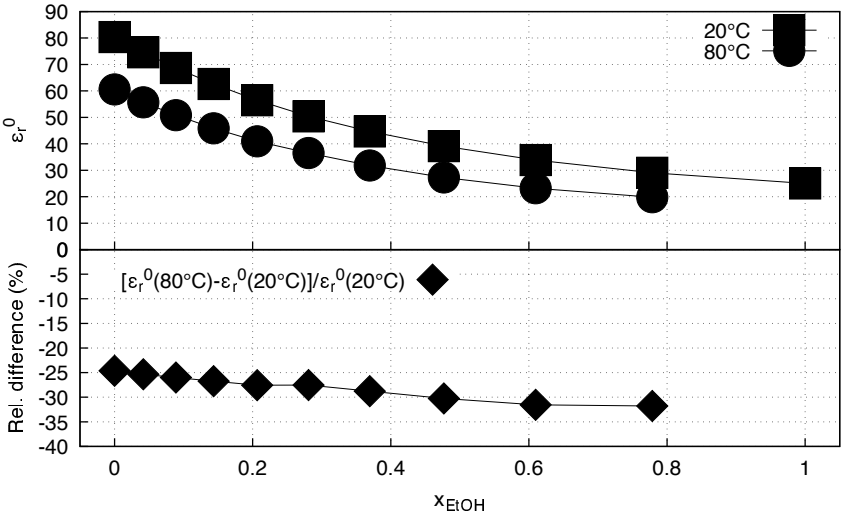

Figure S7: (Top panel) Static relative permittivity vs molar fraction of ethanol x_{EtOH} at ambient pressure and 20°C (squares) and 80°C (disks), data taken from Ref. 3. (Bottom panel) Difference in static relative constant between 20°C and 80°C as a function of the molar fraction of ethanol x_{EtOH}.

Influence of pressure on the static relative permittivity of the solvents

All the syntheses are performed in an autoclave so when the temperature increases the pressure increases too. From the data presented in reference 4 the pressure effect on the static relative permittivity can be plotted. The pressure decreases when ethanol molar fraction increases for a given temperature (25°C) at ambient pressure (1 bar) as well as at

higher pressure (200 bars) (Figure S8). This effect is negligible (variation of about 0.75% to 2.5%) even up to 200 bars (which is 3 times more than the maximum pressure in our experiments), compablack to the influence of x_{EtOH} (Figure S7) or temperature (Figure S9).

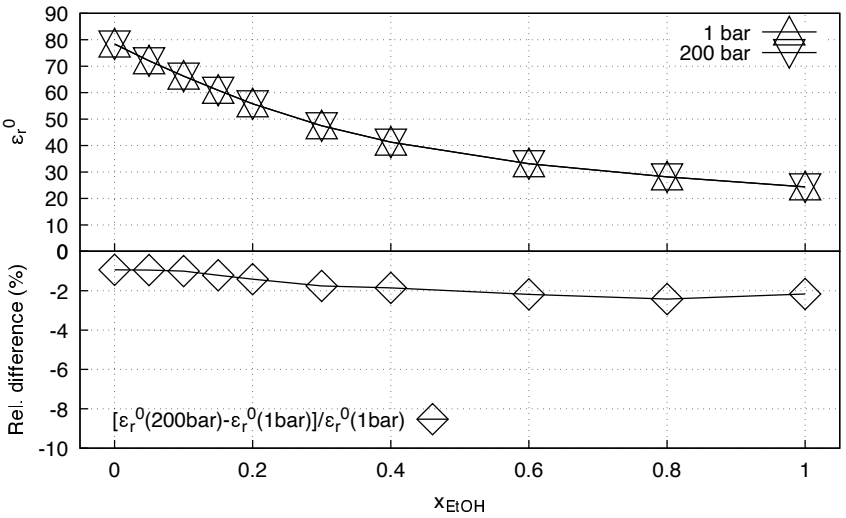

Figure S8: Static relative permittivity under two different pressures vs the molar fraction x_{EtOH} at 25°C (top panel), data taken from Ref. 4 and its relative variation between the two pressures (bottom panel).

However our experiments are performed at higher temperatures (150 to 250°C), giving rise to a pressure increase in the range of 10 to 70 bar (see Fig.7). The question therefore remains as to whether the increase of temperature and thus the increase of pressure has an influence on the decreasing total relative permittivity values at these higher pressures. Data from Ref. 5 about pure water allow to plot the static permittivity values versus the temperature at three different pressures (10, 50 and 100 bar) (Figure S9).

Figure S9 shows that over the range of the synthesis temperatures and under the generated pressures, the static relative permittivities undergo essentially the same decrease. This tendency for pure water can be extended to the ethanol-water mixtures using figures S7 and S8, in this cases the final static dielectric constant will be lower than for pure water.

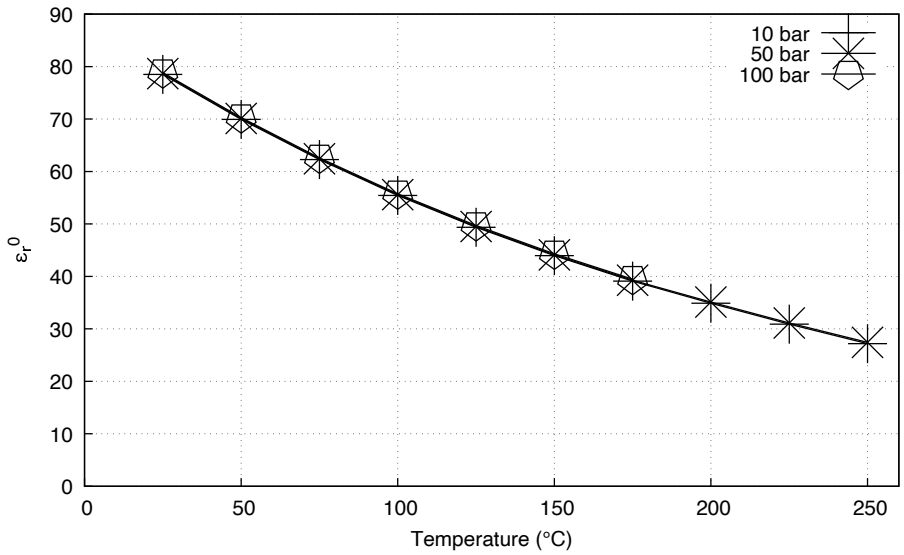

Figure S9: Static relative permittivity of pure water as a function of temperature under three different pressures. Plotted from the data in Ref. 5.

Characterization of the $BaTiO_3$ nano-objects synthesized at the end of the heating stage.

At the end of the heating stage, $BaTiO_3$ is formed but the nano-objects have not yet adopted their final, thermodynamically stable, morphology. Fig.S10 shows the XRD diagram for the synthesis product in E60W40 at the end of the heating ramp up to 250°C. This shows that $BaTiO_3$ is indeed formed before the high-temperature plateau starts.

Fig.S11 shows the SEM images of $BaTiO_3$ nano-objects synthesized in E60W40, enabling the comparison between the morphology of the nano-objects at the beginning (left) and end (right) of the 24 hours temperature plateau. Some nano-tori remain on the beginning of the plateau (indicated by the white arrow), whereas they have changed their shape during the temperature plateau (right).

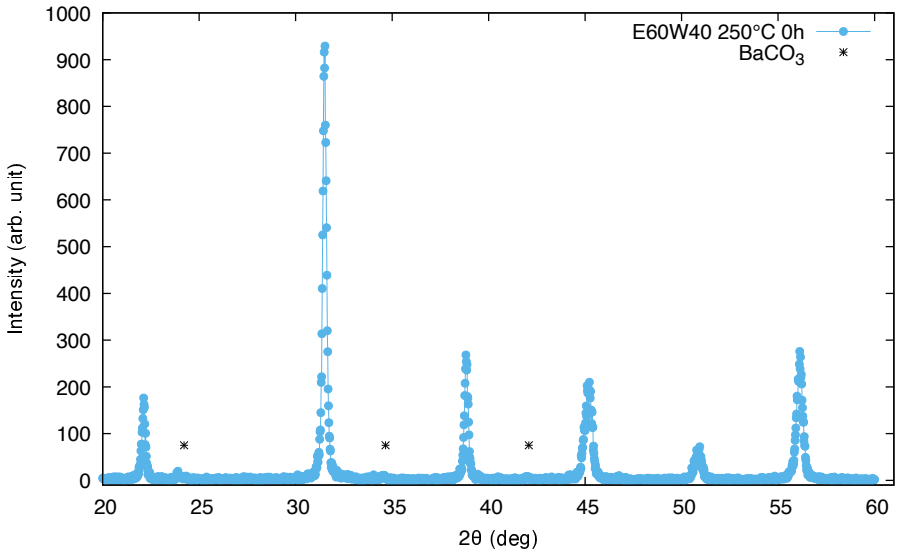

Figure S10: XRD pattern of $BaTiO_3$ synthesized with E60W40 solvent quenched to room temperature after having been heated to 250°C.

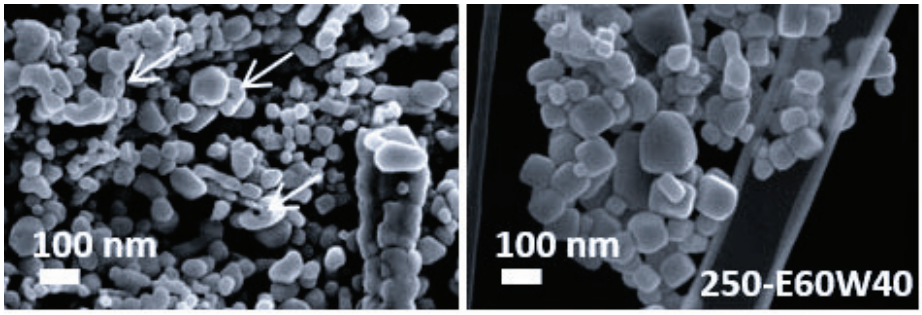

Figure S11: SEM images of synthesized $BaTiO_3$ in the E60W40 solvent quenched to room temperature after having been heated to 250°C (left), and after 24h at 250°C (right). White arrows indicate remaining nano-tori.

References

(1) Ávila, H. A.; Ramajo, L. A.; Reboredo, M. M.; Castro, M. S.; Parra, R. Hydrothermal synthesis of BaTiO3 from different Ti-precursors and microstructural and electrical properties of sintered samples with submicrometric grain size. *Ceramics International* **2011**, *37*, 2383–2390.

(2) Langford, J. I.; Wilson, A. J. C. Scherrer after sixty years: A survey and some new results in the determination of crystallite size. *Journal of Applied Crystallography* **1978**, *11*, 102–113.

(3) Åkerlöf, G. Dielectric constants of some organic solvent-water mixtures at various temperatures. *Journal of the American Chemical Society* **1932**, *54*, 4125–4139.

(4) Morlyoshi, T.; Ishii, T.; Tamai, Y.; Tado, M. Static Dielectric Constants of Water + Ethanol and Water + 2-Methyl-2-propanol Mixtures from 0.1 to 300 MPa at 298.15 K. *Journal of Chemical and Engineering Data* **1990**, *35*, 17–20.

(5) Uematsu, M.; Frank, E. U. Static Dielectric Constant of Water and Steam. *Journal of Physical and Chemical Reference Data* **1980**, *9*, 1291–1306.